Int. J. Electrochem. Sci., 11 **(2016)** 9295 – 9306, doi: 10.20964/2016.11.27

International Journal of ELECTROCHEMICAL SCIENCE
www.electrochemsci.org

Characterization of Zeolitic Imidazolate Framework–derived Polyhedral Carbonaceous Material and its Application to Electrocatalyst for Oxygen Reduction Reaction

Kyo Sung Park[1,†], Seon-ah Jin[1,†], Kang Hee Lee[1,], Junho Lee[2], Inyong Song[2], Byoung-Sun Lee[2], Sookyung Kim[3], Jeongsoo Sohn[3], Chanho Pak[4], Gunha Kim[5], Seok-Gwang Doo[1], Kyungjung Kwon[5,*]*

[1] Energy Material Laboratory, and [2] Analytical Engineering Group, Samsung Advanced Institute of Technology, 130 Samsung-ro, Yeongtong-gu, Suwon, Gyeonggi-do, Korea
[3] Urban Mine Department, Korea Institute of Geoscience and Mineral Resources, 124 Gwahang-no, Yuseong-gu, Daejeon, Korea
[4] Institute of Integrated Technology, Gwangju Institute of Science and Technology, Gwangju, Korea
[5] Department of Energy & Mineral Resources Engineering, Sejong University, Seoul, Korea
[*]E-mail: kanghee.lee@samsung.com, kfromberk@gmail.com
†These authors contributed equally to this work.

Received: 1 July 2016 / *Accepted:* 26 August 2016 / *Published:* 10 October 2016

A porous carbonaceous material is synthesized by direct carbonization of zeolitic imidazolate framework-67 (ZIF-67). A series of analytical tools such as scanning/transmission electron microscopy, gas chromatography/mass spectroscopy, thermogravimetric analysis, nitrogen adsorption, X-ray diffraction, X-ray photoelectron spectroscopy and 3D tomography are conducted for the characterization of the prepared carbonaceous material (ZIF-C). ZIF-C has a well-defined concave dodecahedral shape, and its chemical composition, surface area and electrical conductivity substantially depend on carbonization temperature. ZIF-C heat-treated at 800ºC (ZIF-C-800) shows a typical nitrogen adsorption-desorption isotherm of mesoporous materials with unimodal pores around 2 nm and sufficiently high electrical conductivity comparable to that of carbon nanotubes. ZIF-C-800 has Co metal particles wrapped by graphene layers on the walls of the interior open channels, and its framework is composed of Co-N, C-N species and C-C networks. ZIF-C-800 also displays the highest oxygen reduction reaction catalytic activity among ZIF-C treated at various temperatures, and its feasibility as cathode electrocatalysts for fuel cells is demonstrated by confirming the single cell performance.

Keywords: zeolitic imidazolate framework, mesoporous material, fuel cell, electrocatalyst, oxygen reduction

1. INTRODUCTION

In the last several decades, the structure and property of carbonaceous materials have been widely researched [1-4]. Their properties usually originate from the continuous sp2-hybrid C-C covalent bonding as well as the reduced amount of defects due to their nanoscale size [5]. Moreover, their relatively high specific surface area is very useful in many applications [6]. In the meantime, these carbonaceous materials can have diverse design in accordance with their raw materials and synthesis processes [7, 8]. Depending on their structures and textural properties, carbonaceous materials have various applications such as Li-ion battery anode, Li-air battery cathode, supercapacitor electrode, gas storage, display, and support for catalyst [9-13].

The excellent electrical property and porous microstructure of many carbonaceous materials allow themselves to serve as electrode materials for fuel cells. It is well known that fuel cells have higher efficiency in energy conversion compared to other renewable energy conversion devices [14]. Among various types of fuel cells, polymer electrolyte membrane fuel cells (PEMFCs) have the advantages of quick start-up and high durability because of its lower operating temperatures than other types of fuel cells [15]. However, PEMFCs require expensive electrocatalysts such as platinum, making their commercialization difficult. Therefore, cost-effective alternative electrocatalysts have been intensively developed particularly for oxygen reduction reaction (ORR) in PEMFCs.

Herein are reported porous polyhedral carbonaceous materials with unimodal pores, high electrical conductivity, and promising catalytic activity for ORR. As a precursor can determine the shape, size and porosity of the resulting carbonaceous material, we deliberately chose zeolitic imidazolate framework (ZIF), a type of metal-organic framework (MOF), as a carbon precursor [16-18]. ZIF has a well-defined porous structure due to its high crystallinity [19-21], and is thermally stable enough to maintain its framework and porosity even after high-temperature treatment. ZIF has been used as precursors of ORR electrocatalysts in some reports [22-28]. In this study, we focus on the investigation of structure of ZIF-derived carbonized materials and the active site for ORR. A ZIF precursor (ZIF-67) consisting of imidazolates and Co^{2+} is converted to ZIF-C, which is a carbonaceous material containing Co-N_x moieties and C-N species. The morphology and microstructure of ZIF-C were investigated by various characterization techniques, and its electrocatalytic performance was characterized by ORR activity.

2. EXPERIMENTAL

2.1. Materials

2-Methylimidazole (MeIm, 99%, Aldrich) and $Co(NO_3)_2 \cdot 6H_2O$ (99%, Aldrich) were used for synthesizing ZIF-67. Methanol (Duksan Science) was used as a solvent. Ketjen black carbon (KB300J, Akzo Co.) and single-wall nanotubes (SW-CNT, Iljin Co.) were employed as commercial references to evaluate electrical resistance.

2.2. Synthetic procedures

ZIF-67 was synthesized by following a modified procedure of ZIF-8 synthesis [20]. MeIm (6.48 g, 79.04 mmol) was dissolved in 400 mL methanol, and $Co(NO_3)_2 \cdot 6H_2O$ (2.93 g, 10.08 mmol) was added into the MeIm solution while stirring. MeIm existed in excess quantity, as the stoichiometric ratio between MeIm and $Co(NO_3)_2 \cdot 6H_2O$ was 2:1. The solution turned deep purple and turbid within 10 minutes. The mixture was further stirred overnight, and the synthesized nanocrystals were subsequently separated from the solution by centrifugation. The collected nanocrystals were washed with methanol 3 times. Then they were further immersed in methanol for 3 days, with daily change of fresh methanol. The nanocrystals were eventually recovered by centrifugation and dried in 100ºC overnight (yield: 32%).

ZIF-67 was carbonized to form ZIF-C. Various carbonization temperatures (e.g., 500, 800, and 1100ºC) were used to investigate the characteristics of the resulting ZIF-C. The sample codes (ZIF-C-500, ZIF-C-800 and ZIF-C-1100) refer to their respective carbonization temperatures. A tubular furnace was used for carbonization in N_2 flow. The ramping rate and treatment time were 100 ºC/h and 2 h, respectively. Afterwards the furnace was cooled down to room temperature. The prepared ZIF-C was finally ground into fine powders in a mortar. The synthetic procedure is shown schematically in Fig. 1.

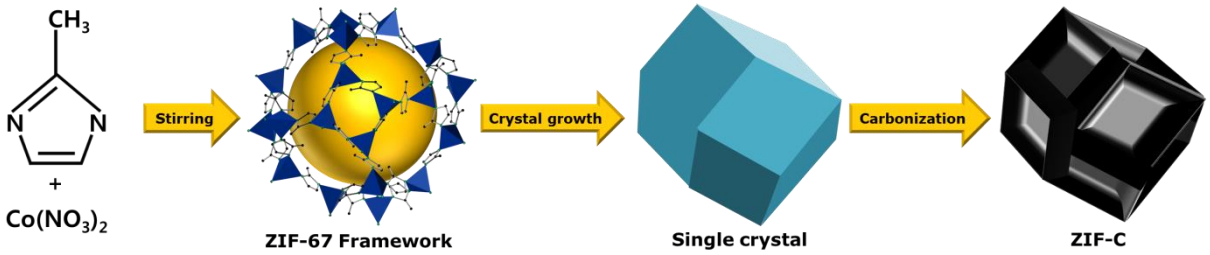

Figure 1. Schematic illustration of the synthetic procedure of ZIF-C.

2.3. Characterization

The obtained ZIF-67 was analyzed with powder X-ray diffraction (XRD, Cu Kα, λ = 0.15406 nm, D8 Advance, Bruker) and the pattern was compared with simulation. Scanning electron microscopy (SEM) analysis was performed on a Hitachi S5500 scanning electron microscope operated at 10-30 kV. Transmission electron microscopy (TEM) images and energy dispersive X-ray spectroscopy spectra were acquired by using FEI Osiris 200 kV TEM. X-ray photoelectron spectroscopy (XPS) measurements were performed with a Micro-XPS using the monochromatic Al Kα source (27.7 W power and 100 μm beam size). Nitrogen adsorption experiments were performed using a Micromeritics Tristar 3000 system. The surface area of the samples was calculated using the Brunauer–Emmett–Teller (BET) equation, while the pore size distribution was estimated by the Barrett–Joyner–Halenda method from adsorption branch of the isotherms. In order to visualize 3D Z-contrast, high angle annular dark field scanning transmission electron microscopy was conducted for

tomography tilt series acquisition and 3D reconstruction was performed by using FEI Inspect3D Software. Thermogravimetric analysis (TGA) was conducted with TA Q5000 instrument from room temperature to 1000°C under nitrogen flow. Resolved gas during the heat treatment for ZIF-67 was identified by gas chromatography/mass spectroscopy (GC/MS, AGILENT Co.).

The electrochemical properties of ZIF-C were evaluated with a rotating disc electrode (RDE) system (Princeton Applied Research). Glassy carbon was used as a substrate for the working electrode, and the catalyst ink was made according to our previous papers [29, 30]. The ZIF-C catalyst was dispersed in an aqueous suspension using ultrasonication, and the suspension was pipetted onto the glassy carbon substrate. Nafion solution (0.05 wt%, Aldrich) was pasted on the top of the dried catalyst powder. The electrolyte was 0.1 M $HClO_4$ aqueous solution. Linear scan voltammetry was performed for the ORR evaluation in the oxygen-saturated electrolyte at the scan rate of 5 mV/s. The potentials throughout this study are reported with respect to the reversible hydrogen electrode (RHE).

A polybenzoxazine-based membrane was used for the single-cell evaluation of electrocatalysts, and the amount of phosphoric acid in the membrane was controlled by immersing the dry membrane in phosphoric acid at 80ºC for a few hours [29, 30]. The cathode catalyst layer was composed of the synthesized electrocatalyst and polyvinylidene fluoride (PVDF) binder. The anode catalyst layer consisted of carbon-supported Pt-Ru alloy (Tanaka Kikinzoku Kogyo) and PVDF. The catalyst loadings of the cathode and anode for Pt were approximately 3.0 and 1.0 mg/cm^2, respectively. For comparison purpose, a single cell adopting Pt_3Co/C (Tanaka Kikinzoku Kogyo) cathode catalyst layer was also fabricated. Dry hydrogen gas for the anode and dry air for the cathode were used for single cell operation conducted at 150ºC.

3. RESULTS AND DISCUSSION

The synthesized ZIF-67 has morphology of well-defined rhombic dodecahedron, as shown in Fig. 2(a). Note that the rhombic dodecahedron was formed because each Co atom was connected to four imidazolate linkers to form a tetrahedron in ZIF. From the clear facets of the crystal we deduce that the single crystals were successfully synthesized. The XRD pattern of prepared ZIF-67 was perfectly matched to the simulated one as confirmed in Fig. 2(b). More details on the characterization of ZIF-67 have been described elsewhere [20]. In the SEM images of ZIF-C (Fig. 2(c)-(f)), the rhombic dodecahedral morphology was maintained after carbonization except for slight volume shrinkage. The frames of ZIF-C particles were strictly conserved with concaved facets. The observed length of the frames in Fig. 2(e) and 2(f) was from 100 nm to 150 nm.

In order to understand the structural changes from ZIF-67 to ZIF-C during carbonization, the thermal decomposition of ZIF-67 was investigated by TGA and GC/MS. The inset of Fig. 3 shows that the thermal decomposition of ZIF-67 starts at 450ºC and continues up to 1000ºC. Since carbon dioxide (CO_2), acetonitrile (CH_3CN), and hydrogen cyanide (HCN) were detected in chromatogram at 560ºC, the imidazole groups are presumed to be partially decomposed into the gaseous products during thermal treatment. Methyl imidazolate was detected in GC as well. Total weight loss obtained in TGA was approximately 70 wt%.

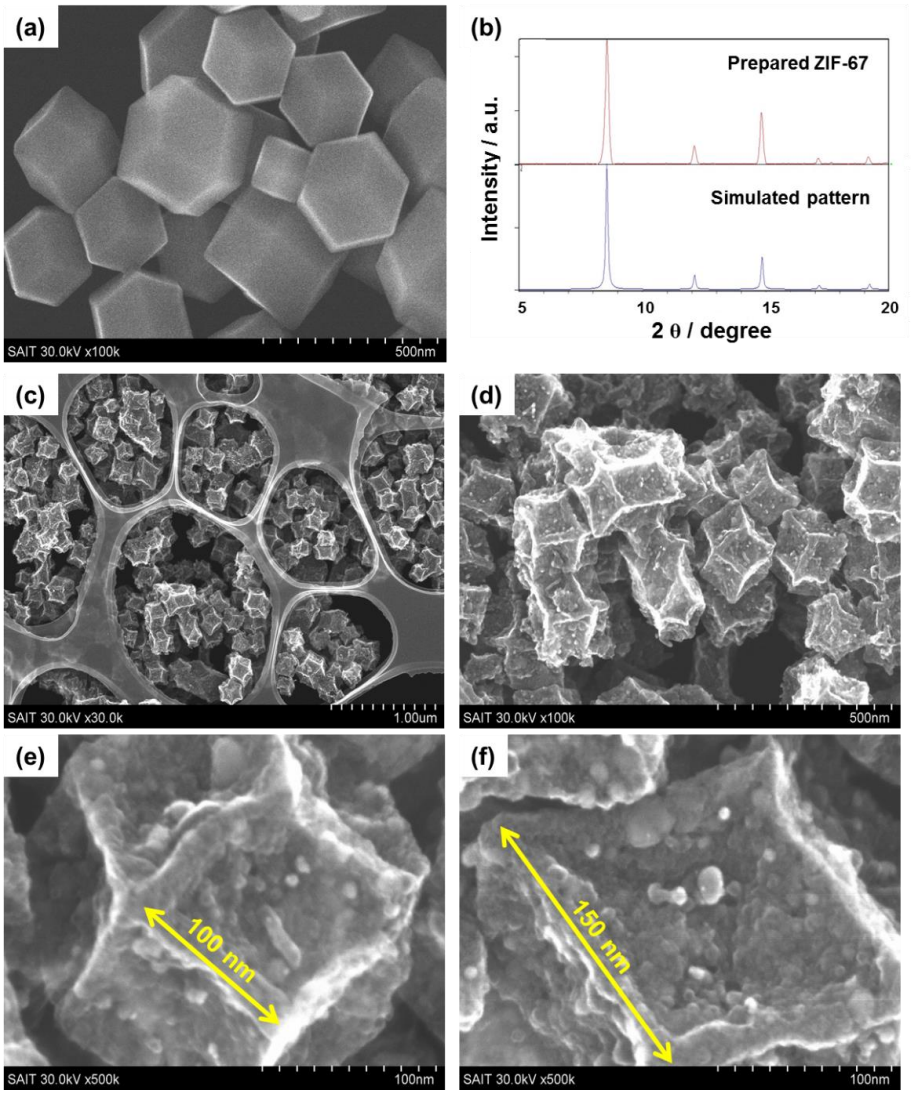

Figure 2. (a) SEM images and (b) experimental and simulated XRD patterns of ZIF-67. (c), (d), (e), and (f): SEM images of ZIF-C under different levels of magnification.

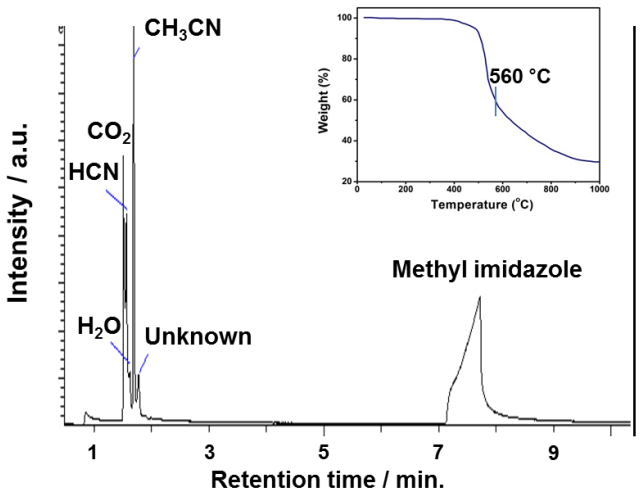

Figure 3. GC/MS analysis of gases from the thermal decomposition of ZIF-67 at 560°C in N_2 flow. Inset: TGA results of ZIF-67 in N_2 flow up to 1000°C.

In this study, it is speculated that structural rearrangement including breaking and rebinding of frameworks occurred during the thermal treatment. A notably high undecomposed weight (30 wt%) was achieved due to the high thermal stability of ZIF-67 [20]. It has been known that the imidazole functional groups could become a precursor of N-doped CNTs [31, 32]. We therefore expect that the C-N as well as C-C bonds in ZIF-C would be formed from the imidazole groups.

Nitrogen adsorption isotherms of ZIF-C carbonized at different temperatures were measured by the BET method (Fig. 4). ZIF-C-500 showed higher N_2 uptake than ZIF-C-800 and ZIF-C-1100. The BET surface area of ZIF-C-500 was calculated to be 1396 m^2/g, while those of ZIF-C-800 and ZIF-C-1100 were 322 m^2/g and 172 m^2/g, respectively.

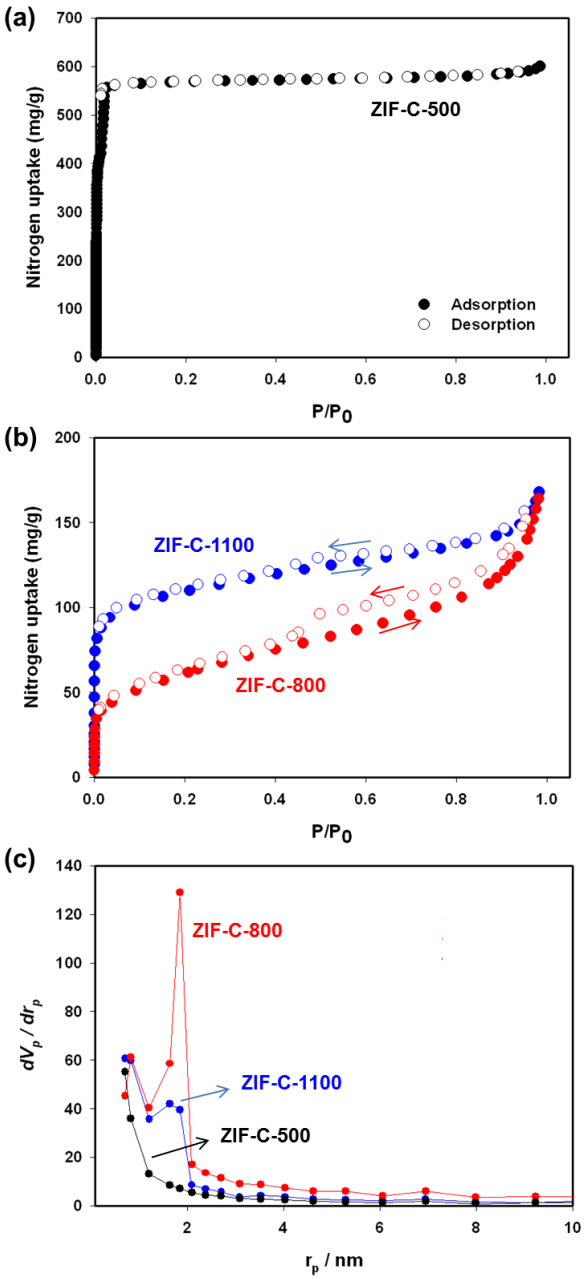

Figure 4. Textural characterization of ZIF-C carbonized at various temperatures. (a), (b) Nitrogen adsorption-desorption isotherm curves. (c) Pore size distribution curves.

We do not expect ZIF-C-500 to be fully carbonized, because the weight loss just starts at this temperature in TGA (Fig. 3, inset). The total pore volume gradually decreased with increasing carbonization temperature from 0.71 cm^3/g to 0.14 cm^3/g and 0.10 cm^3/g for ZIF-C-500, ZIF-C-800 and ZIF-C-1100 respectively as shown in Table 1. Meanwhile, the isotherms of ZIF-C-800 and ZIF-C-1100 showed H2 type hysteresis, which is a typical phenomenon in mesoporous materials, in Fig. 4(b). In Fig. 4(c), a peak in the pore size distribution for ZIF-C-800 and ZIF-C-1100 implied that uniform pores of which size is 1.85 nm were formed through the carbonization process. Contrary to reports [23, 33] on the synthesis of template-free porous carbon using cross-linked polymers where unimodal pores were not formed, the introduction of ZIF-67 as a carbonizing precursor as in our study is a demonstration of making well-defined porous carbonaceous materials without template.

Table 1. Textural, elemental and electrical properties of ZIF-C carbonized at 500, 800 and 1100ºC.

Sample	BET surface area (m^2/g)	Pore volume (cm^3/g)	C, H, N Elements analysis (wt%)			*Electrical resistance (mΩ/□)
			C	H	N	
ZIF-C-500	1396	0.71	42.7	4.8	25.1	N.A.
ZIF-C-800	322	0.14	47.8	1.1	6.0	1.94
ZIF-C-1100	172	0.10	56.2	0.08	0.69	1.74

*The samples were pelletized under the pressure of 1,400 psi, and then measured by a 4-point probe. (Reference carbon materials: Ketjen black 77.67mΩ/□, single-wall carbon nanotube 4.86mΩ/□)

The result of element analysis of prepared ZIF-C is summarized in Table 1. The amounts of hydrogen and nitrogen decrease whereas that of carbon increases with increasing carbonization temperature. The cobalt content is estimated at 43–45 wt% in all the ZIF-C samples. The presence of metallic Co would contribute to the electrical conductivity of ZIF-C. Since the conductivity is an important property for an electrode material in PEMFC, the electrical resistance of ZIF-C was measured, and the value for ZIF-C-1100 (1.74 mΩ/□) is lower than for ZIF-C-800 (11.94 mΩ/□). The resistances of all the ZIF-C samples, especially ZIF-C-1100, were lower than that of Ketjen black, and comparable to that of single-wall carbon nanotubes (4.86 mΩ/□). The decent electrical property of ZIF-C could be related to Co metal on frameworks and regular Catalan shape that can be closely packed while being pelletized.

The nanostructure of ZIF-C was further investigated by HR-TEM and XRD to understand its morphology and electrical property. As shown in Fig. 5, the microstructure of ZIF-C consists of Co metal nanoparticles 5–20 nm in diameter with several layers of graphene wrapped on the outside. The metallic Co particles were identified by XRD analysis, which is shown in Fig. 5(b). The Co-imidazolate framework of ZIF seems to be converted to Co metal nanoparticles and Co-N-C frameworks. The Co metal nanoparticles with carbon shell are attributed to the resolution of Co^{2+} and imidazoles in ZIF-67, and subsequent growth of the reduced Co metal nanoparticles during carbonization. The thickness of the carbon shell was in the range of 1–2 nm, corresponding to 3–6 graphene layers. Graphene layers are known to form on the surface of transition metals by contact with

hydrocarbon gases at high temperatures. Such carbon deposition on transition metal catalysts has been mainly observed in water-gas shift reaction where it often leads to catalyst deactivation. However, the graphene shells with a large amount of carbon and nitrogen atoms as well as Co-N_x moieties would be active for ORR.

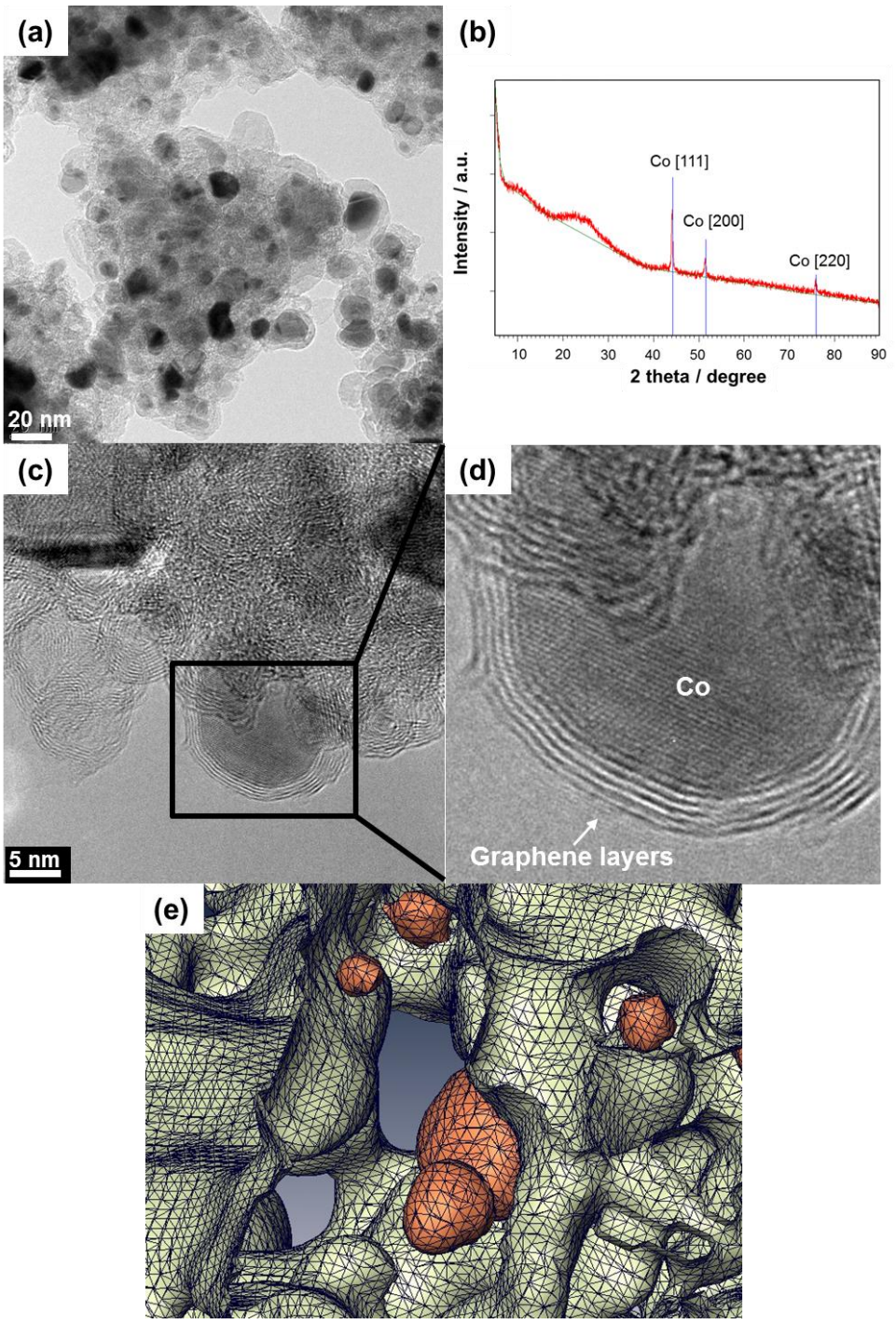

Figure 5. Characterization of microstructure of prepared ZIF-C-800. (a) TEM image. (b) XRD pattern. (c) and (d) Magnified TEM images, showing cobalt particles enveloped in graphene layers. (e) 3D tomography of the developed channels inside ZIF-C-800 (red particle: Co metal).

3D tomography measurement was performed to investigate the internal structure of ZIF-C. As shown in Fig. 5(e), there are open channels connected to each other in the ZIF-C solid. The mutually interconnected channels can offer facile mass transfer for both reactants and products. The Co metal particles were found on the walls of the open channels of ZIF-C. The framework of ZIF-C would be composed of Co-N_x moieties and C-C networks created from undecomposed component.

XPS analysis was conducted for ZIF-C-800 to evaluate its surface composition and the oxidation state of each element. As shown in Fig. 6, carbon, nitrogen, oxygen and cobalt were detected, with the calculated atomic composition of 88.9%, 4.5%, 4.6%, and 2.0%, respectively. More specifically, the N1s peak can be deconvoluted into three different N species: pyridinic N at 398.7 eV, graphitic N at 400.8 eV and an unknown N species at 404.5 eV as shown in Fig. 6(b). Among them, major species is the pyridinic N that is known to be more active than other N species for ORR [34]. Co^{2+} peak was detected at 780.6 eV on ZIF-C (Fig. 6(c)), indicating that Co-N_x moieties remained in frameworks, although a considerable portion of Co atoms were converted to Co metal particles. Carbon was slightly oxidized during carbonization as shown in C1s peak (Fig. 6(d)).

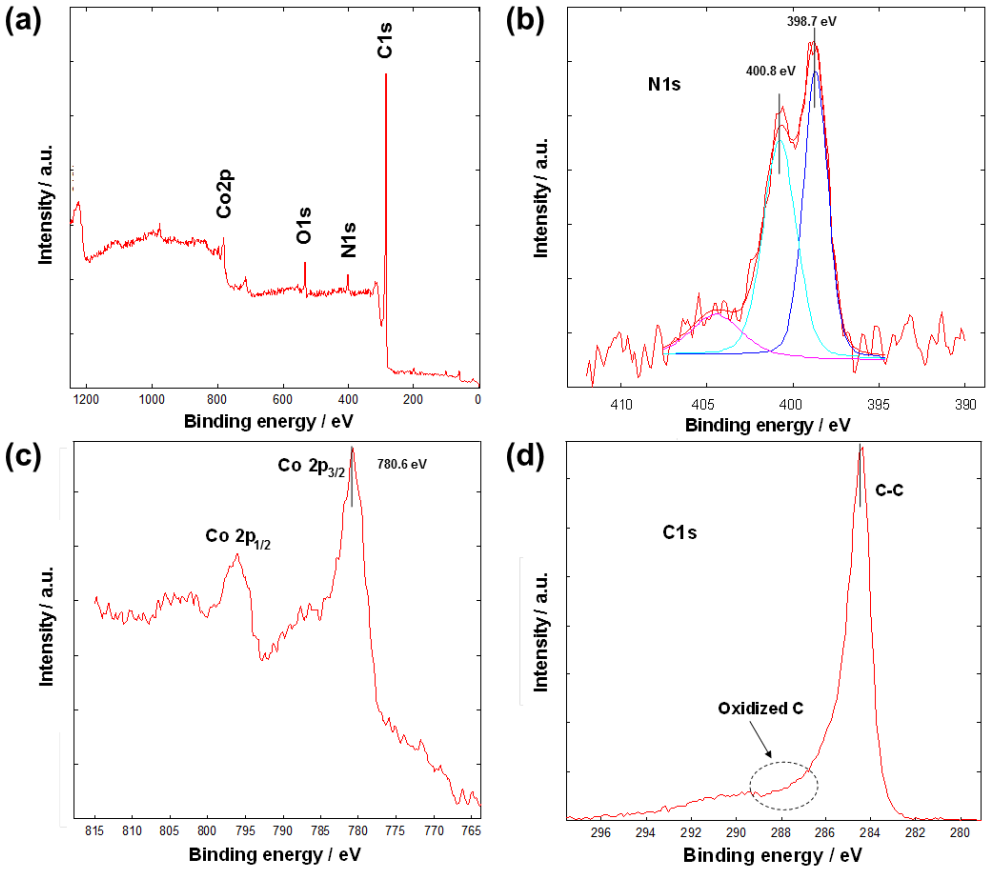

Figure 6. XPS spectra of ZIF-C-800 in (a) full range, (b) N1s, (c) Co2p, and (d) C1s.

The ORR activity of ZIF-C was investigated aiming at an application to catalyst in fuel cells. Research on non-precious metal electrocatalysts for ORR has been actively carried out in order to replace the Pt-based precious metal electrocatalysts since Jasinski found that Co-N_4 moiety in cobalt

phthalocyanine showed activity for ORR [35]. Recently, several reports have been published regarding metal-N-C ORR electrocatalysts that were prepared from MOF [22, 23]. The ORR activity of ZIF-C was investigated by RDE method in 1 M $HClO_4$ solution saturated with oxygen. A comparison of ORR activity using ZIF-C carbonized at various temperatures is shown in Fig. 7. The ORR current of ZIF-C-500 is negligible due to insufficient carbonization. The best ORR activity is obtained from ZIF-C-800, indicating complete carbonization which results in the maximization of active sites in the carbon network. A relatively lower ORR activity was observed in ZIF-C-1100, possibly due to shrinkage of its surface area from heat shock at 1100ºC.

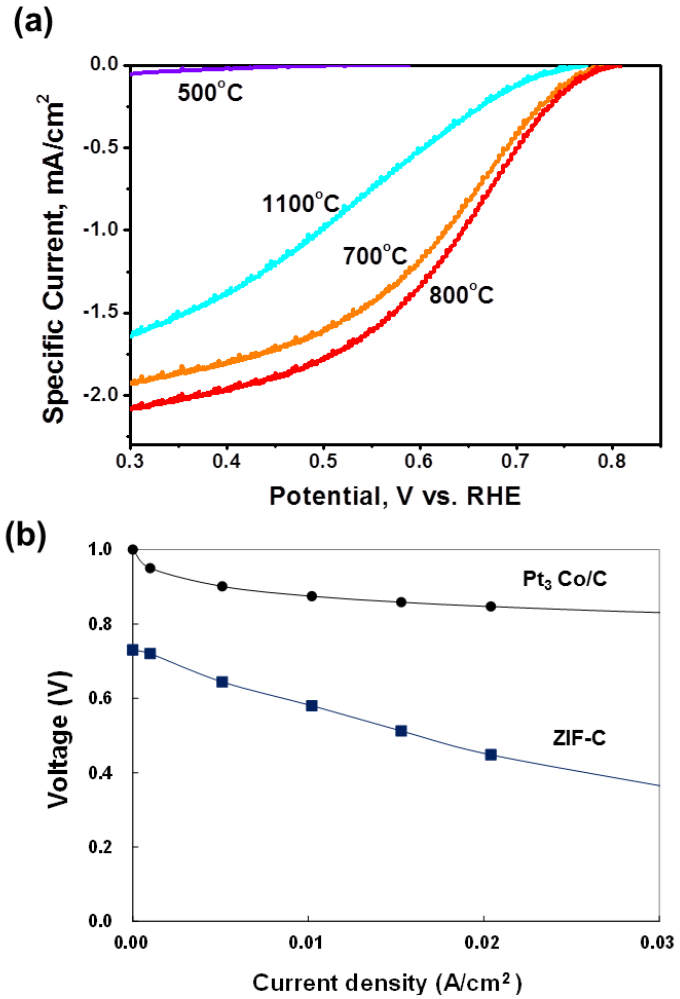

Figure 7. ORR activity of ZIF-C. (a) ORR currents from RDE test, using ZIF-C carbonized at various temperatures. (b) MEA performances of ZIF-C-800 and Pt_3Co/C.

We further assessed the membrane electrolyte assembly (MEA) performance of ZIF-C as cathode catalyst of PEMFC at 150ºC. Compared to commercial Pt_3Co/C, which is one of the most active ORR catalysts, ZIF-C showed lower performance in PEMFC as shown in Fig. 7(b). In contrast with Pt_3Co/C, a lower open circuit voltage (OCV) and a higher ohmic overpotential were observed for ZIF-C. The ORR onset potential of ZIF-C around 0.8 V was realized as an OCV value of MEA in between 0.7 V and 0.8 V whereas it seems that less dense ZIF-C than Pt_3Co/C needs a thicker

electrode for securing enough amount of active catalytic sites, which in turn incurs a higher ohmic overpotential at electrodes.

Finally we consider the active catalytic site of ZIF-C. The Co-N_x moieties as an active site would be formed in the frameworks after carbonization as suggested by Ma et al. [22]. On the other hand, Co metal particles were stuck on the wall of open channels in ZIF-C. C-N species would exist in graphene layers around the Co metal particles, becoming a different active site created from decomposed imidazolates as confirmed by GC/MS analysis. The graphene layers are speculated to contain many C-N sites due to their large surface area. Interaction between the Co metal particles and the C-N species in graphene layers with respect to electrochemical reaction could not be deduced in this study. Further investigation is needed to fully understand the active site in Co-N-C electrocatalyst and improve its activity for ORR.

4. CONCLUSIONS

A carbonaceous material, ZIF-C, was prepared from ZIF-67 through carbonization process. The dodecahedron frame of ZIF-67 remained more or less after carbonization up to 1100ºC. The high electrical conductivity of ZIF-C measured from pelletized sample is believed to be due to the existence of Co metal and the regular dodecahedron structure. Its porous structure would promote the ORR activity by a facile mass transfer of reactant and product. Catalytic activity of ZIF-C for ORR was observed in RDE and PEMFC MEA tests. The Co-N_x moieties in frameworks and C-N species in graphene layers on the Co metal particles would play a role of active site for ORR. Besides the ORR catalytic activity, the well-defined structure, high electrical conductivity and unimodal pores of ZIF-C could make it useful for many other electrochemical applications.

ACKNOWLEDGEMENT
This study was supported by the R&D Center for Valuable Recycling (Global-Top R&BD Program) of the Ministry of Environment.

References

1. C. Niu, E. K. Sichel, R. Hoch, D. Moy and H. Tennent, *Appl. Phys. Lett*., 70 (1997) 1480.
2. S. J. Tans, A. R. Verschueren and C. Dekker, *Nature*, 393 (1998) 49.
3. M. Zhang, S. Fang, A. A. Zakhidov, S. B. Lee, A. E. Aliev, C. D. Williams, K. R. Atkinson and R. H. Baughman, *Science*, 309 (2005) 1215.
4. B. Demczyk, Y. Wang, J. Cumings, M. Hetman, W. Han, A. Zettl and R. Ritchie, *Mater. Sci. Eng. A*, 334 (2002) 173.
5. R. Liao, Z. Tang, T. Lin and B. Guo, *ACS Appl. Mater. Inter.*, 5 (2013) 2174.
6. S. Arayachukeat, T. Palaga and S. P. Wanichwecharungruang, *ACS Appl. Mater. Inter.*, 4 (2012) 6808.
7. T. Bhuvana, A. Kumar, A. Sood, R. H. Gerzeski, J. Hu, V. S. Bhadram, C. Narayana and T. S. Fisher, *ACS Appl. Mater. Inter.*, 2 (2010) 644.
8. B.-S. Lee, S.-B. Son, K.-M. Park, G. Lee, K. H. Oh, S.-H. Lee and W.-R. Yu, *ACS Appl. Mater.*

Inter., 4 (2012), 6702.
9. H.-M. Cheng, Q.-H. Yang and C. Liu, *Carbon*, 39 (2001) 1447.
10. Z. Hamoudi, B. Aissa, M. A. El Khakani and M. Mohamedi, *Int. J. Electrochem. Sci*., 7 (2012) 12227.
11. W. Choi, D. Chung, J. Kang, H. Kim, Y. Jin, I. Han, Y. Lee, J. Jung, N. Lee and G. Park, *Appl. Phys. Lett.*, 75 (1999) 3129.
12. J. Wu, M. Agrawal, H. A. Becerril, Z. Bao, Z. Liu, Y. Chen and P. Peumans, *ACS Nano*, 4 (2009) 43.
13. H. Wang, J. K. Keum, A. Hiltner, E. Baer, B. Freeman, A. Rozanski and A. Galeski, *Science*, 323 (2009) 757.
14. B. Bae, K. Miyatake and M. Watanabe, *ACS Appl. Mater. Inter.*, 1 (2009) 1279.
15. B. Narayanamoorthy, K. K. R. Datta, M. Eswaramoorthy and S. Balaji, *ACS Appl. Mater. Inter.*, 4 (2012) 3620.
16. H. Nakagawa, K. Watanabe, Y. Harada and K. Miura, *Carbon*, 37 (1999) 1455.
17. K. Miura, J. Hayashi and K. Hashimoto, *Carbon*, 29 (1991) 653.
18. Q. Zeng, D. Wu, C. Zou, F. Xu, R. Fu, Z. Li, Y. Liang and D. Su, *Chem. Commun*., 46 (2010) 5927.
19. K. S. Park, Z. Ni, A. P. Côté, J. Y. Choi, R. Huang, F. J. Uribe-Romo, H. K. Chae, M. O'Keeffe and O. M. Yaghi, *Proc. Natl. Acad. Sci. U.S.A.*, 103 (2006) 10186.
20. R. Banerjee, A. Phan, B. Wang, C. Knobler, H. Furukawa, M. O'Keeffe and O. M. Yaghi, *Science*, 319 (2008) 939.
21. A. Phan, C. J. Doonan, F. J. Uribe-Romo, C. B. Knobler, M. O'keeffe and O. M. Yaghi, *Acc. Chem. Res*., 43 (2010) 58.
22. S. Ma, G. A. Goenaga, A. V. Call and D. J. Liu, *Chem. Eur. J*., 17 (2011) 2063.
23. E. Proietti, F. Jaouen, M. Lefèvre, N. Larouche, J. Tian, J. Herranz and J.-P. Dodelet, *Nat. Commun*., 2 (2011) 416.
24. D. Zhao, J.-L. Shui, L. R. Grabstanowicz, C. Chen, S. M. Commet, T. Xu, J. Lu and D.-J. Liu, *Adv. Mater*., 26 (2014) 1093.
25. X. Wang, J. Zhou, H. Fu, W. Li, X. Fan, G. Xin, J. Zheng and X. Li, *J. Mater. Chem. A*, 2 (2014) 14064.
26. H. M. Barkholtz, L. Chong, Z. B. Kaiser, T. Xu and D.-J. Liu, *Catalysts*, 5 (2015) 955.
27. L. Shang, H. Yu, X. Huang, T. Bian, R. Shi, Y. Zhao, G. I. N. Waterhouse, L.-Z. Wu, C.-H. Tung and T. Zhang, *Adv. Mater*., 28 (2016) 1668.
28. Z. Li, M. Shao, L. Zhou, Q. Yang, C. Zhang, M. Wei, D. G. Evans and X. Duan, *Nano Energy*, 25 (2016) 100.
29. K. H. Lee, K. Kwon, V. Roev, D. Y. Yoo, H. Chang and D. Seung, *J. Power Sources*, 185 (2008) 871.
30. K. Kwon, K. H. Lee, S.-A. Jin, D. J. You and C. Pak, *Electrochem. Commun*., 13 (2011) 1067.
31. E. N. Nxumalo, V. P. Chabalala, V. O. Nyamori, M. J. Witcomb and N. J. Coville, *J. Organomet. Chem*., 695 (2010) 1451.
32. K. Ghosh, M. Kumar, T. Maruyama and Y. Ando, *J. Mater. Chem*., 20 (2010) 4128.
33. C. Zou, D. Wu, M. Li, Q. Zeng, F. Xu, Z. Huang and R. Fu, *J. Mater. Chem*., 20 (2010) 731.
34. N. P. Subramanian, X. Li, V. Nallathambi, S. P. Kumaraguru, H. Colon-Mercado, G. Wu, J.-W. Lee and B. N. Popov, *J. Power Sources*, 188 (2009) 38.
35. R. Jasinski, *Nature*, 201 (1964) 1212.